NUREG/CR-0263
SAND78-0299
R7

DEBRIS BED STUDIES AND EXPERIMENTS AT SANDIA LABORATORIES

J. B. Rivard

Sandia Laboratories

NUREG/CR-0263
SAND78-0299
R-7

DEBRIS BED STUDIES AND EXPERIMENTS AT SANDIA LABORATORIES

J. B. Rivard

Date Published: July 1978

Sandia Laboratories
Albuquerque, New Mexico 87185
operated by
Sandia Corporation
for the
U. S. Department of Energy

Prepared for
Division of Reactor Safety Research
Office of Nuclear Regulatory Research
U. S. Nuclear Regulatory Commission
Washington, D.C. 20555
Under Interagency Agreement DOE 40-550-75
NRC FIN No. A1181

ABSTRACT

An initial experiment simulating a 58 mm thick LMFBR fuel debris bed has been performed in liquid sodium in which the UC_2 particles composing the bed were internally heated by nuclear fission. The experiment was performed in the Annular Core Pulse Reactor (ACPR), as part of Sandia Laboratories' program examining the safety of advanced reactors. Supporting research included experiments utilizing other power sources and simulated debris and coolants, analysis and modeling, and auxiliary measurement of material properties and interactions.

The specific power attained during the in-reactor experiment ranged up to about 1 kW/kg of UO_2 while the bulk sodium temperatures ranged up to 838 K. The bed was 102 mm in diameter and had a porosity (sodium volume fraction) of 0.48. The particulate UO_2 used was irregular in shape in 100 to 1000 μm sizes. Thermocouples were located at two levels within the particle bed. With one exception, temperatures within the bed (which ranged up to 1008 K) behaved in a manner characteristic of thermal conduction. The magnitude of the effective conductivity at 900 K is about one-half the value for the sodium alone.

The particle-to-fluid interface does not appear to offer significant resistance to heat transfer at these power levels. The heat transfer behavior of the bed was quite reproducible, and edge effects appeared to be small. Extrapolation of the results to beds of larger lateral extent appears feasible. The limiting condition for this type of bed heat transfer probably does not occur prior to the occurrence of boiling at or near the bottom of the bed.

CONTENTS

ILLUSTRATIONS

TABLES

DEBRIS BED STUDIES AND EXPERIMENTS AT SANDIA LABORATORIES

INTRODUCTION

An accident in a Liquid Metal Fast Breeder Reactor (LMFBR) in which molten core material is suddenly quenched with subcooled liquid sodium could result in extensive fragmentation and dispersal of fuel and structural material as subcritical beds of frozen particulate debris within the reactor vessel. Because this debris will continue to generate power due to the decay of contained fission products, retention of the debris is threatened if the generated heat is not removed. Therefore, the initial safety question is the capacity which a debris bed may have for transfer of the decay heat to overlying liquid sodium by natural processes--i.e., without the aid of forced circulation of the coolant through the bed.

Up to the present time, all experiments concerning debris bed behavior either have used substitute materials (e.g., sand and water) or have employed real reactor materials, but atypical heating methods. In order to properly simulate the heat transfer behavior typical of decay-heated fuel material, it is necessary that the heat be generated primarily within the oxide fuel material rather than within the sodium coolant or external to the container. The debris bed studies program[1] which has been initiated at Sandia Laboratories includes the first experiments in which decay heating is accurately simulated in real reactor materials, under realistic conditions. In these experiments within the Annular Core Pulse Reactor (ACPR), steady-state fission heating of enriched oxide fuel material in liquid sodium is used to simulate the decay heating

of the debris. Supporting research includes experiments utilizing other power sources and simulated LMFBR debris and coolants, analysis and modeling, and auxiliary measurements of material properties and interactions. This program is responsive to the needs of the Division of Advanced Reactor Safety Research of the U. S. Nuclear Regulatory Commission.

The initial series of three experiments in the ACPR, designated D-1, D-2, and D-3, Table 1, is designed to provide basic reference data on the cooling capacity of representative debris beds under typical post-accident reactor conditions. Important issues to be addressed include: (1) whether or not bed depth is an influencing parameter on cooling capacity, (2) what the influence of sodium subcooling is, and (3) how the results correlate with the results of non-reactor experiments and with analytical treatments. Besides providing this frame of reference for safety assessment, it is expected that an initial understanding of bed phenomena will be gained, the details of which can be determined in future experiments. Finally, the initial series will provide experience in this type of experimentation in the ACPR, thus reducing effort, timescales and expense on future experiments.

This report covers the program results through the performance of the first in-reactor experiment (D-1) in May, 1977. Results of the D-2 and D-3 experiments, as well as all post-test examination results, will be published separately.

TABLE I

Debris Bed Experiment Parameters

Parameter	D-1	D-2	D-3
Bed Loading, kg $(UO_2)/m^2$	300.	600.	899.
Total Fuel, kg (UO_2)	2.432	4.866	7.292
Bed Depth, mm	58	106.*(99.-113.)	158.
Max. Specific Power kW/kg (UO_2)	1.0	1.28	0.43
Sodium Mass, kg	2.837	2.924	3.131
Gas Volume @ 473K, m^3	0.98 (10^{-3})	1.00 (10^{-3})	1.07 (10^{-3})
Sodium Volume Fraction in Bed	0.48	0.43	0.43
Bulk Sodium Temperatures, K	673,773,823,838	673,873	673,773,873
Max. Observed Temperature, K	1007.	1188.	1265.

*Average value, bed surface inclined

REACTOR DESCRIPTION

The ACPR[2] is a light-water cooled and moderated pool-type reactor which utilizes U-ZrH fuel/moderator which is based on TRIGA experience. The reactor's outstanding feature is a dry, 229 mm diameter central cavity which is provided for the irradiation of experiments. The cavity is surrounded by approximately 150 fuel elements 381 mm long arranged in an annulus. The reactor may be operated either in the pulse or steady-state mode. In the steady-state mode utilized for the debris bed experiments described herein, it is capable of a maximum power of 600 kW.

EXPERIMENT DESCRIPTION

Figure 1 is a mechanical schematic of the overall debris bed experiment system. The principal functions performed by the apparatus shown are: 1) containment of the fuel and sodium in a sealed stainless steel or Inconel vessel in the center of the ACPR; 2) removal of heat generated within the experiment; 3) control of the sodium temperature within the experiment canister; and 4) measurement of the power developed by the experiment. The two major systems shown in the Figure are the Helium Cooling Loop and the Experiment Package.

Experiment Package

The experiment package houses and insulates the capsule containing the fuel and sodium, supports and positions the experiment in the reactor, and conveys the helium, air and instrumentation cables which support the experiment. It is a 7.8 m long assembly

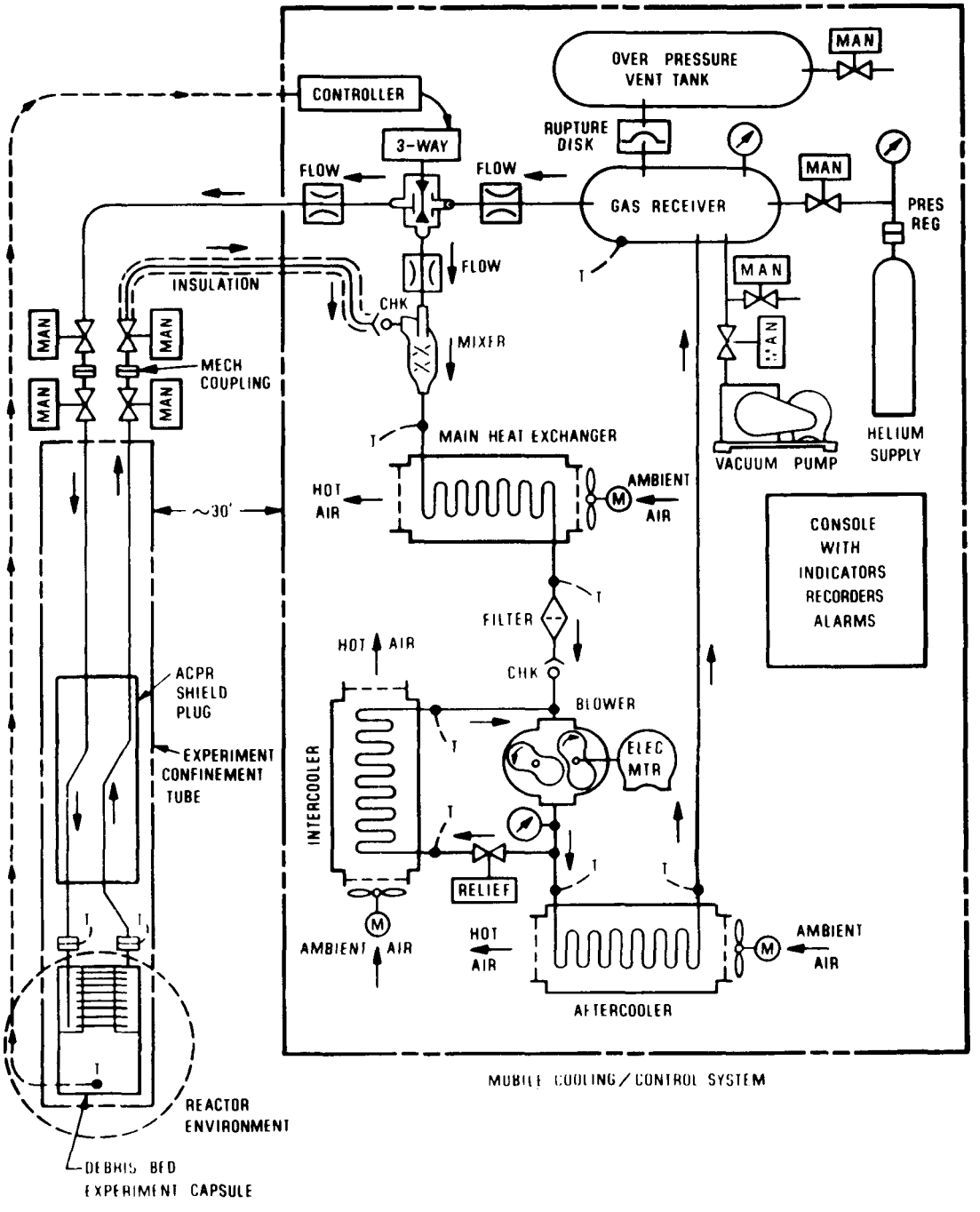

FIGURE 1 - Debris bed experiment schematic.

which is inserted vertically into the experiment access tube of the ACPR. It is made up of three major parts: the upper, intermediate, and lower sections. The upper section of the package contains (at the upper end) the system for connecting to the piping extensions of the helium cooling loop, air-cooling connections, and a junction box for instrumentation connections. It is approximately 4.5 m long, contains the helium and air piping, insulation, structural supports, and neutron shielding material. The intermediate section contains helium, air, and instrumentation connections at both ends where it joins with the upper and lower sections. Besides piping, this 2.5 m long section contains structural supports, insulation, and a segmented stainless steel gamma shield. The lower section connects to it and houses the experiment itself. This section is about 1.0 m long and consists of the bed canister, the sodium-helium heat exchanger, shroud assembly, helium vessel, and outer housing together with diagnostic and safety instrumentation (Figure 2).

The debris bed experiment capsule contains the bed which is composed of fully enriched particulate UO_2, a quantity of sodium and an inert gas. The capsule is composed of two sections: the lower 102 mm inside diameter canister which contains the bed, and the upper heat exchanger section. The capsules for tests D-1, D-2, and D-3 differ in length to accommodate different sized beds. The capsules are made from 304 stainless steel (D-1) or Inconel 617 (D-2, D-3) with a nominal wall thickness of 3.2 mm. The upper (heat exchanger) section contains, at its lower end, a circular

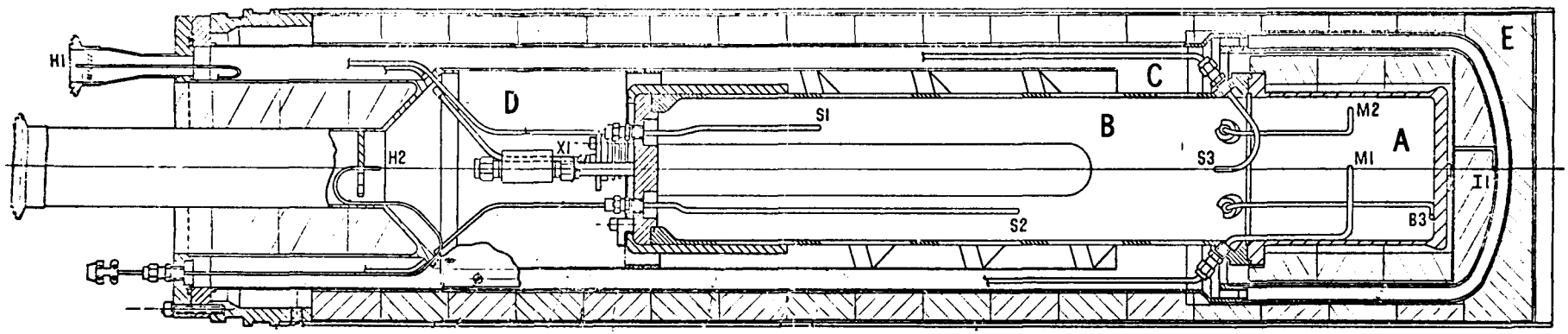

FIGURE 2 - Debris bed experiment capsule. The debris bed is located in the sealed chamber at A, with the overlying sodium at B. Cool helium enters at C and exits at D after passing through the helical cooling passages. Typical solid insulation is shown at E.

arrangement of sealing glands for thermocouples, a central cooling section, and an upper expansion plenum section. The capsule is positioned inside the helium vessel which is in turn surrounded by insulation and the outer shell.

Instrumentation consists of 10 thermocouples located internally and on the outside surface of the bottom of the debris bed capsule, and 2 pressure transducers which sense the pressure inside the capsule. The thermocouples are Inconel sheathed, type K (chromel-alumel) and are of the closed-end design. Number, end design, and location are given in Table II. The pressure transducers are the Kaman Sciences Corporation variable impedance, eddy-current type in which both uniform temperature effects and radiation effects are nulled out.

Table II

Type K, 3.2 mm O.D. Inconel Sheathed Thermocouples

Number	Junction Type	Location
2	Grounded, Special Pad	Weld onto outside bottom of capsule
2	Grounded	Inside bottom of capsule
1	Isolated	Inside bottom of capsule
2	Isolated	Mid-bed
3	Isolated	Three heights in overlying sodium

Additional instrumentation includes two 1.6 mm O.D. grounded junction, type K thermocouples located in the inlet and exhaust helium streams, respectively. These are used to measure one required component (ΔT) in the determination of the power being removed by the helium cooling system from the experiment. Also included is a type K thermocouple located on the inner bottom of the helium vessel below the capsule.

Helium Heat Transfer Loop[3]

Helium, flowing externally through the heat exchanger section of the capsule, is used to remove the heat generated within the debris bed. The heated helium then flows through insulated piping to a portable cooling loop located outdoors which is used to dissipate the heat.

Figure 1 shows this system schematically. The rate of heat transfer from the experiment is controlled by diversion of some of the helium flow to a pipe which bypasses the experiment. The amount of helium which is bypassed is determined by the position of the three-way control valve. This valve is positioned by a signal from a central controller which senses deviations from the bulk sodium set-point temperature and automatically provides a compensating output. The objective of this control system is to maintain a constant bulk sodium temperature in the experiment while operating at various heat removal rates.

The loop has a maximum flow rate of 38 g/s at a pressure of 276 kPa and was designed to handle heat loads of up to 20 kW.

The helium is circulated by a positive displacement blower powered by an 11.2 kW electric motor.

Determination of the heat being removed by the helium from the debris bed capsule is accomplished by measurement of the helium ΔT mentioned above and the mass flow rate of helium to the experiment. These measurements are subsequently combined to form the product which is proportional to the power being removed from the experiment. The mass flow measurement is accomplished by use of instrumented orifices which supply signals to an on-line analog computer. Final processing of the power information is performed by an on-line digital data acquisition and display system (DADS).[4]

SUPPORTING EXPERIMENTS AND ANALYSIS

Gamma Ray Transport at Boundaries

Application of the results of the debris bed experiments to post-accident heat removal in a LMFBR depends partly upon the adequacy of fission heating as a simulation of fission product decay heating.

For fission-heated fuel particle sizes above 100 μm in size, most of the fission fragment energy is deposited locally, and less than 10 percent direct fission energy transfer into the sodium or experiment boundary can be anticipated.[5] In the LMFBR, where the fuel particles making up the debris bed are being heated by fission product decay, slightly more than half of the energy appears in the form of gamma rays up to about 3 hours after reactor shutdown. Many of these gamma rays are reasonably energetic and some can be expected to escape the debris bed. This has the effect of reducing

the bed power near the bed boundaries and adds internal heating to the materials which form the boundaries of the bed.

One-dimensional transport calculations have been performed to characterize the power redistributions caused by gamma ray escape at boundaries of debris beds.[6] Figure 3 shows the results of a typical calculation in which it was assumed that 50 percent of the decay power appears as gamma-rays while the remainder was uniformly absorbed locally within the fuel region. A gamma energy spectrum which is typical of that occurring during the early stages of fission product decay has been utilized, and the region to the left of the origin contains sodium. For the condition shown, in which the porosity (sodium volume fraction) of the bed is 60 percent, the power level in the iron immediately adjacent to the bed is nearly 25 percent of the average bed power. For less porous beds, the percent power developed in the iron is reduced. However, since the power levels in the adjacent materials are non-trivial, this effect must be considered in the overall evaluation of debris behavior, and in its simulation by fission heating.

Debris Description

Three processes were tried for the production of the UO_2 fuel used in the D-1, D-2, and D-3 experiments to simulate LMFBR debris. In the selected process[7], ceramic grade UO_2 is isostatically pressed into a "green" log which is then crushed. The green fragments are then sieved and high-fired at 2073 K in H_2 for 24 hours and finally crushed. The process yields about 70

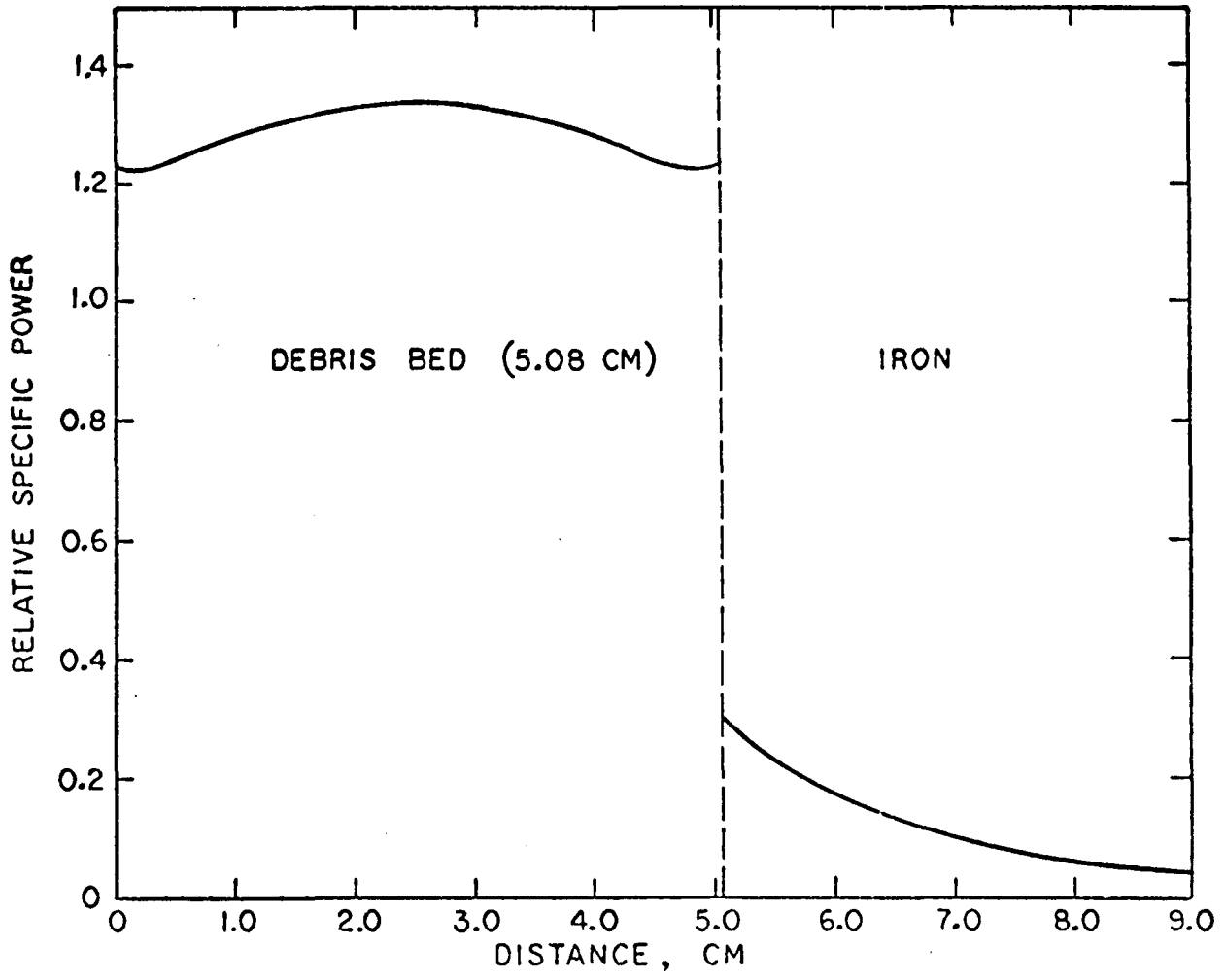

FIGURE 3 - Calculation of power profiles in and adjacent to a 60 percent porous debris bed.

percent particulate in the specified particle size range. The UO_2 is fully enriched in the 235 isotope. The particulate has been characterized by both photomicrography and SEM. Figure 4 is a 40 X photomicrograph showing typical particles, while Figure 5 shows the lower central portion of Figure 4 at a magnification of 250 X. The UO_2 has a density of approximately 90% of theoretical and is slightly sub-stoichiometric (1.98 O/U). The particle size distribution for the D-1 experiment is shown in Figure 6. The "mean particle diameter" as described in Ref. 14 is about 500 μm, while the average (arithmetic mean) particle size is about 220 μm.

Permeability of Simulated Debris

The permeability of unenriched UO_2, prepared by a process similar to that described above, and in a similar size distribution, has been measured at the University of Arizona.[8,9] Argon was used as the fluid medium at flow rates giving superficial velocities of from 2. to 14. mm/s through a bed of 10-cm diameter. Nominal bed depths of 20, 40, 60, 80, and 120 mm were used. The permeability, κ, as measured, was a function of both bed depth and amount of settling (compaction) of the bed.

Thus, κ increased from 90 to 180 darcys for lightly settled beds of 20- to 130-mm depth while, for considerably more settled beds, κ ranged from 80 to 125 darcys for the same bed depths. The permeability increased with increasing bed depth. The permeability was not influenced greatly by the fluid velocity in a given

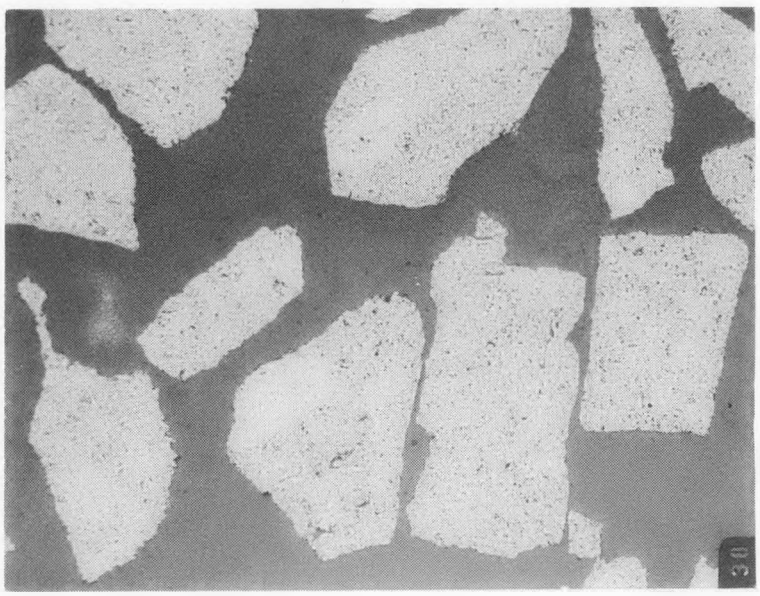

SSO-2 40X

FIGURE 4 - 40X photomicrograph of typical UO_2 particles.

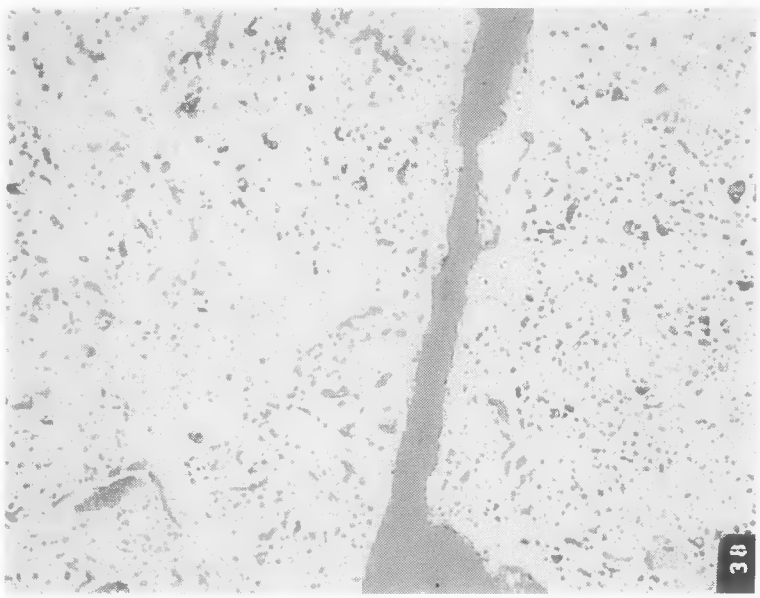

SSO-2 250X

FIGURE 5 - 250X photomicrograph of lower central position of Figure 4.

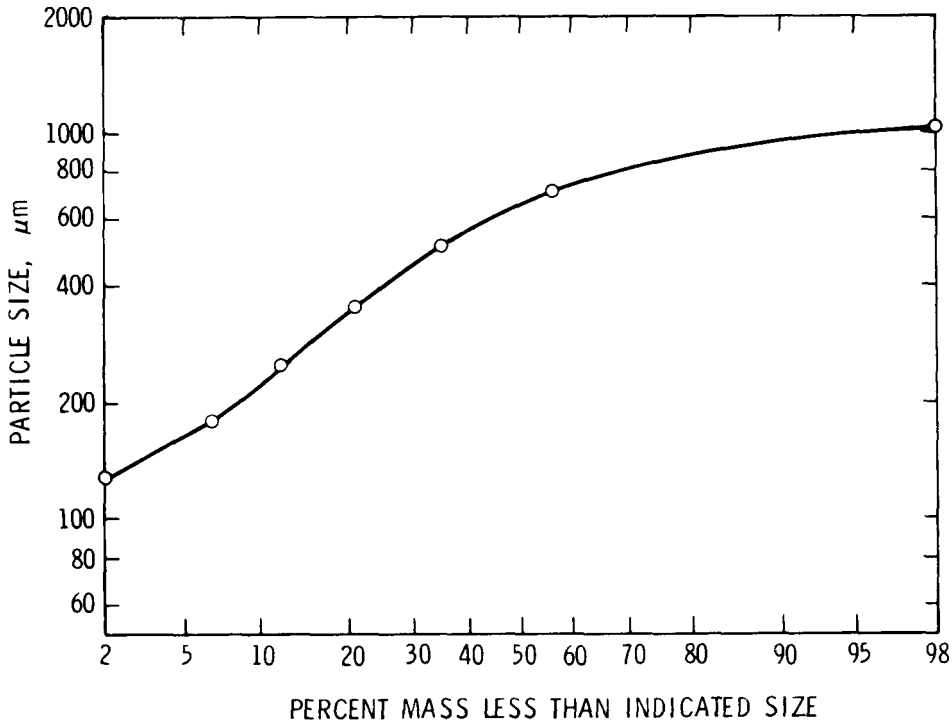

FIGURE 6 - UO_2 particle size distribution (D-1).

configuration although, at the lowest velocities, there was some reduction in κ as compared with higher velocity values.

The surprising increase in permeability with increasing bed depth has been determined to be due to the method of forming the bed. The UO_2 was poured into the chamber of the permeability apparatus from a constant height, and the lower layers of the bed were therefore agitated by gravity-driven impact forces to a greater extent than were the upper layers of the bed. This led to the situation where the pressure drop gradient is much lower in the upper layers of the bed, and the lowest layers had a high pressure drop gradient corresponding to a well-packed bed. Thus, as deeper beds were formed, the average pressure drop gradient, decreased and thus the permeability κ, increased with increasing bed depths. The phenomena were repeatable.

Debris Bed Analysis and Experiments

Analysis and laboratory experiments have been performed[10] in order to provide a composite picture of debris bed behavior in all heat transfer regimes: conduction, single-phase convection, and two-phase boiling convection. An analytical model of a single-phase convective roll cell was derived by an approximate technique which leads to the result $Nu = 0.177\ Ra^{0.5}$ and $Ra_c = 32$, which agrees well with the work of Buretta and Berman,[11] and Sun.[12]

These results form the theoretical framework for Figure 7, which shows the results of four steady-state experiments conducted by electrical heating of salt water in beds of sand. All boundaries

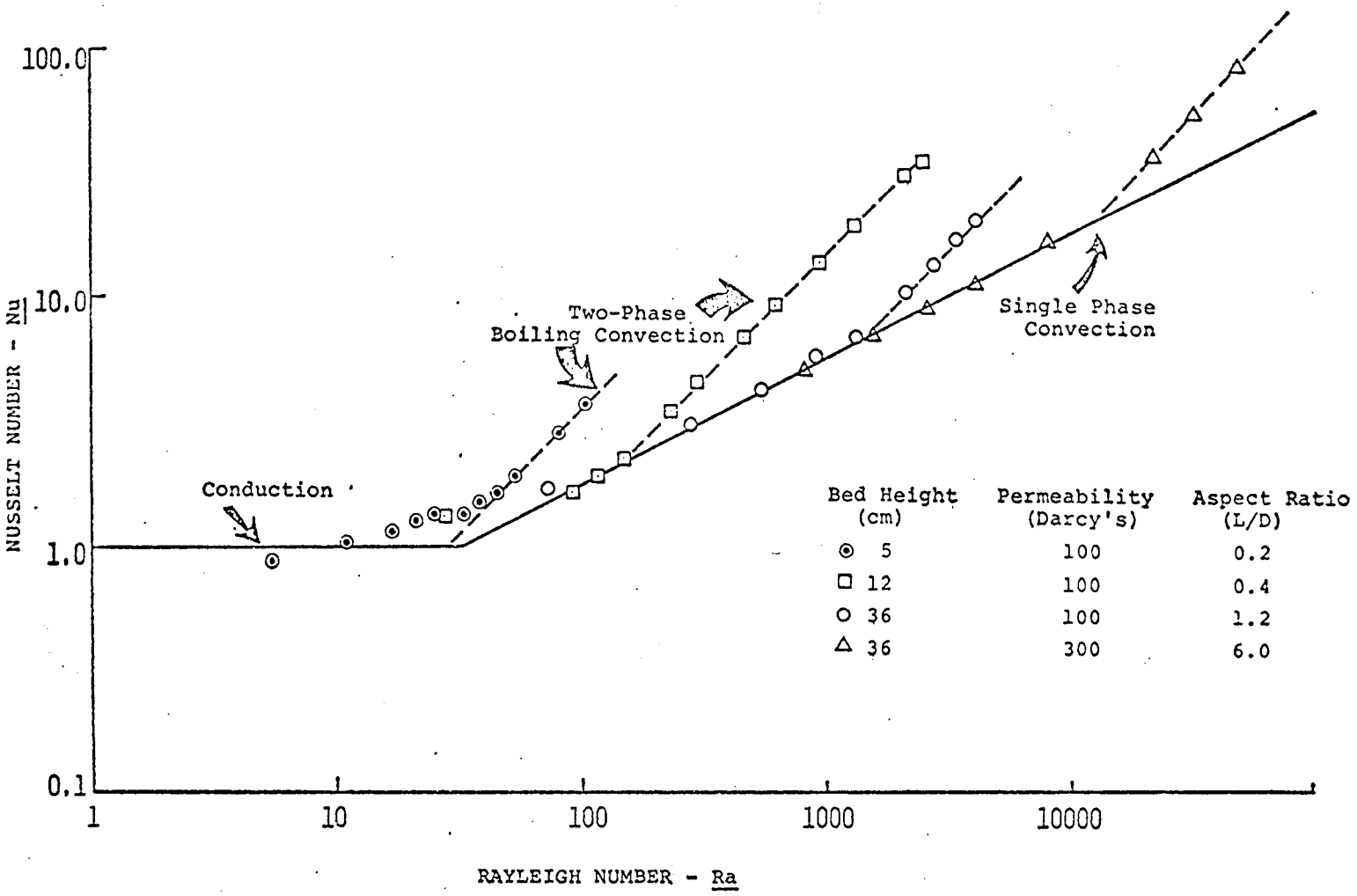

FIGURE 7 - Heat transfer for a heat-generating porous bed cooled from above.

were insulated except the upper surface which was maintained at a constant temperature by a heat exchanger. The family of dashed lines extends from the solid conduction and single phase convection line (with a break at $Ra_c = 32$) into the boiling regime. The shallow bed experienced boiling before the onset of single-phase convection. Near the limit of dryout of the beds, a quasi-steady cycle of liquid expulsion and reflooding was observed. It is thought that this may be a consequence of heating the fluid rather than the particulate.

An overall energy balance can be made near the top of a deep two-phase bed, assuming that the bed is cooled primarily by latent heat transport. If continuity and Darcy's law are applied to liquid downflow and vapor upflow, the heat flux $Q_v L(1-\epsilon)$ is seen to depend on the ratio between the upflow and downflow areas. An upper bound may be derived by selecting the value of this parameter which maximizes the heat flux:

$$Q'_v L(1-\varepsilon) = \frac{(C_\ell \Delta T/\mathcal{L} + 1)}{\left[1 + \sqrt{\nu_\ell/\nu_v}\right]^2} \frac{\rho_\ell g \kappa \mathcal{L}}{\nu_v}$$

Here, ΔT represents the quantity $T_{Boiling} - T_C$.

This model predicts the proper order of magnitude for dryout heat fluxes as reported by several researchers.

Neutron Transport Analysis

One- and two-dimensional neutron transport calculations have been performed[13] to characterize the power deposition and the power

deposition profiles within realistic debris bed experiment configurations in the ACPR. The initial efforts, using DTF-IV, were directed towards the selection of optimum materials and thicknesses for filters to harden the neutron spectrum within the bed. The calculations showed that about 1 mm of natural boron plus 1.7 mm of tantalum produced the best profiles with the least overall power degradation. (It was required that the filter materials be capable of sustained high temperature operation.) With these filters the calculations gave average specific power levels in the largest debris bed (D-3) of approximately 1.25 kW per kilogram of UO_2 at an ACPR power of 600 kW and a maximum-to-average specific power ratio of ~1.2.

The local-to-average specific power ratios for the largest debris bed, based on two-dimensional calculations, are shown in Figures 8 and 9. Near the bottom of the experiment (curve A in Figure 8), the radial power profile rises smoothly from an axial minimum to a maximum at the outside radius. Near the top of the experiment (curve B in Figure 8), however, the profile shows a central hump which results from the absence of neutron filter materials above the bed (filter materials surround the outer radius and the bottom of the bed canister only). Figure 9 shows the same peaking effect in the vertical profiles near the upper edge of the bed and also shows a slight central hump which probably reflects the flux peak near the center of the reactor. The profiles in the smaller experiments (D-1 and D-2) will generally be somewhat less peaked.

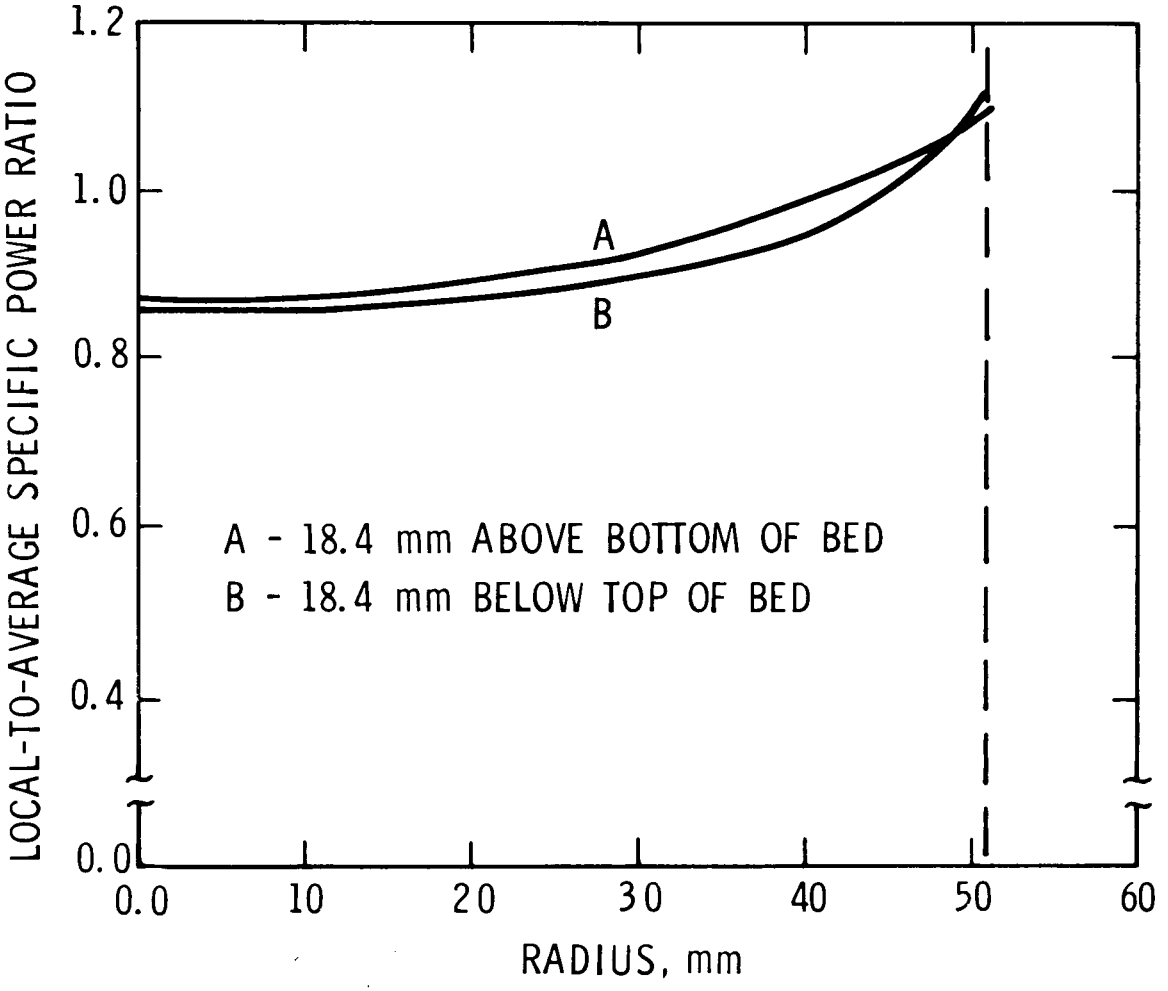

FIGURE 8 - Radial local-to-average specific power ratios.

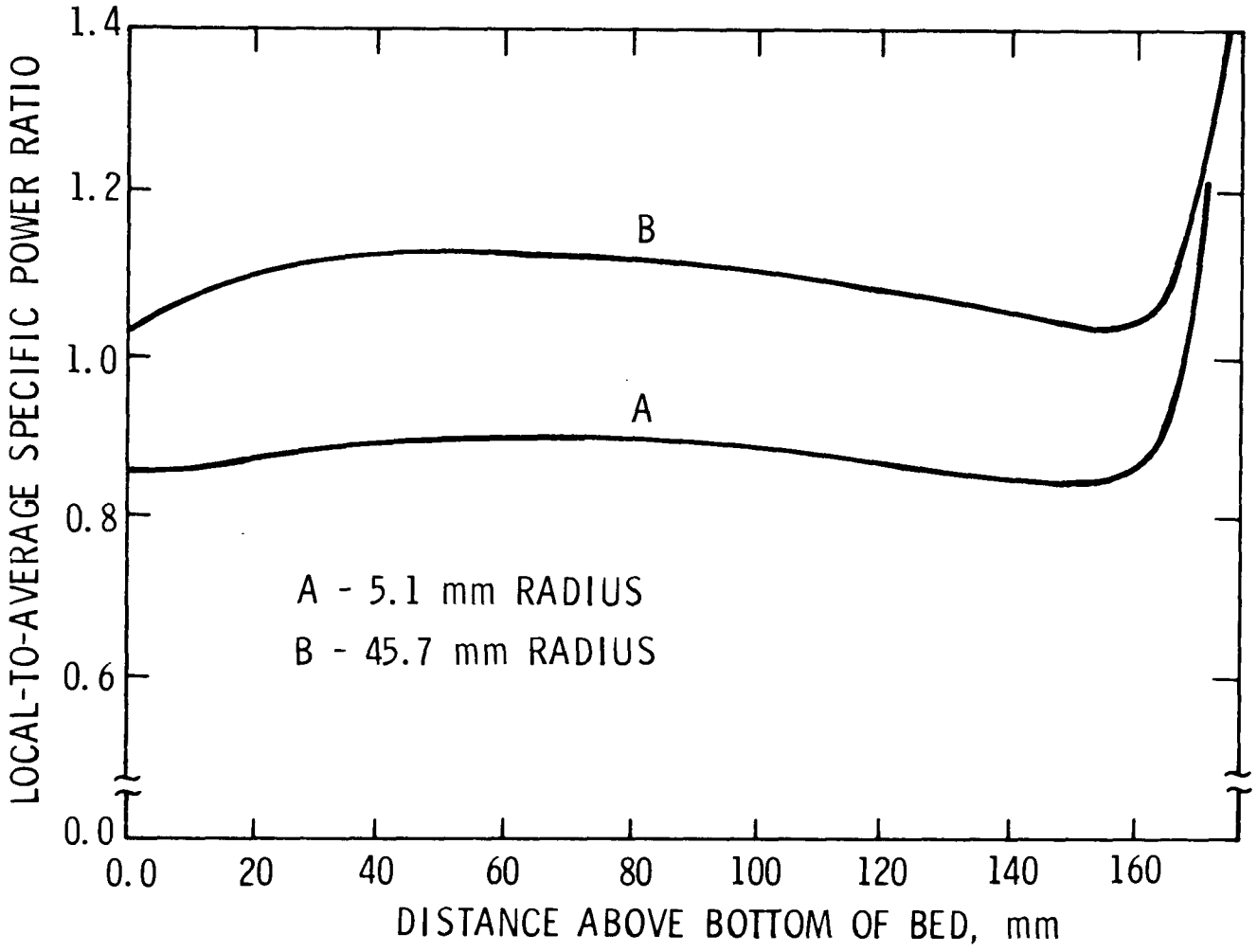

FIGURE 9 - Axial local-to-average specific power ratios.

GENERAL EXPERIMENT PROCEDURE

The first three in-pile experiments utilizing fully-enriched UO_2 particulate in sodium are designated D-1, D-2, and D-3. The experiments are numbered sequentially. Succeeding experiments in this series contain increased amounts of fuel by the increment of 2.432 kg. Since the experiment canister diameter is constant, the depth of the UO_2 beds is increased approximately in proportion to the increase in mass.

Following loading of the experiment package into the reactor, connection to the helium cooling loop, and connection of instrumentation and control cabling, initial checkout of the system is performed and a reactivity measurement is made (cold). Reactivity adjustment to the reactor is made at this time to compensate for the reactivity effect of the experiment.

Following the initial checkout, helium heated by the sodium preheating system is circulated through the experiment package to melt the sodium in the capsule. The reactivity worth of the experiment is then again measured to insure that the melting of the sodium has not significantly changed the reactivity.

After the sodium is fully melted, the sodium preheating operation is halted and the reactor is started up and brought up to a low power level. Checkout of the experiment diagnostics is subsequently performed at low temperatures ($\sim$ 473 K); the helium loop control temperature set point is adjusted upward in steps until the initial bulk sodium temperature is reached. This produces confirmation of

control action and allows checkout of the power diagnostic. The first series of power runs is then made, followed by the second series at the next selected bulk sodium temperature. At each sodium temperature level, the power is initially incremented upward from a low level in steps. At least one-half hour is allowed at each power level to allow equilibration of temperatures within the experiment before data is taken.

Dryout, when it occurs, is signaled by one or more continuously rising thermocouple signal(s) in the UO_2 bed and a corresponding failure to achieve steady-state at a given power level. Upon observation of the signals indicating dryout, the reactor power level is reduced to 10 kW after a suitable observation period. This reduction terminates the transient and allows control of the temperatures to be regained.

The entire run at that sodium temperature is again performed starting at a low power level. This rerun procedure is designed to test the repeatability of the dryout phenomenon.

During dryout, the maximum possible or adiabatic rate of rise of temperature in the UO_2 bed is limited by the experiment power level and by the heat capacity of the UO_2. When the power has has been reduced to 10 kW following dryout, the maximum possible (adiabatic) rise rate of the UO_2 temperature has been reduced to about 4 K per minute so that a 5 minute observation period at this level could result in a maximum temperature rise of only 20 K if stable conditions did not return.

During actual dryout, it is anticipated that the rise rates will be somewhat below the maximum possible values due to failure of the adiabatic assumption and other deviations from the ideal conditions upon which the maximum is based. Therefore, the criterion for dryout and subsequent power reduction to 10 kW is based upon failure to achieve a steady state, rather than upon the achievement of a predetermined rate-of-rise of UO_2 bed temperature. Since dryout is a local effect, the temperatures achieved by the thermocouple(s) indicating dryout conditions are not imposed upon the bulk of the sodium and UO_2. Thus, significant pressurization of the capsule will not occur. On the other hand, propagation of dryout can occur; it would be signaled by an increasing number of bed thermocouple outputs rising and prompt power reduction would then be required to return conditions to equilibrium.

Following the power runs, the reactor is shut down. The experiment temperatures will continue to be lowered by the helium helium cooling loop until they reach the sodium freezing point. A reactivity worth measurement is then performed. The experiment is shut down when the bulk sodium temperature reaches 60°C. The experiment is allowed to radioactively decay for about three days before being removed from the reactor and transferred to radioactive storage. After several months of radioactive decay, the post-experiment examination can be started.

D-1 EXPERIMENT

After joining the canister to the heat exchanger section of the D-1 experiment capsule and effecting a valid seal at this

joint, the 2.43 kg of fully enriched UO_2 was loaded into the canister using a ladle. By lowering each ladle of fuel to a level just above the bed as it was being formed, and then tilting it to to release the fuel, minimum impaction of the bed material was ensured. The resulting bed had an average height of 58 mm and a porosity (sodium volume fraction) of 0.48. Following loading, the capsule was evacuated to a low level vacuum which was maintained for several hours. Then the capsule was heated, and 2.84 kg of liquid sodium was added. To ensure that the bed was not disturbed by the flow of sodium into the vessel, the capsule was tilted slightly so that the sodium would impact the wall of the vessel rather than the bed. However, x-rays taken later (Figures 10, 11) of the capsule showed that some erosion of the bed had occurred on the side where the sodium was directed. Finally, the capsule was pressurized with helium to 34.5 kPa (Abs) at 437 K, and cooled to room temperature.

After the experiment package was fully assembled and lowered into position within the ACPR core, reactivity measurements were performed and the sodium was melted by flowing heated helium through the heat exchanger section, utilizing the helium cooling loop system. When the sodium was fully liquid, the reactor was brought up to a low power, and the heating by the helium was slowly decreased until the experiment was maintained at temperature entirely on its own power, with the helium flow providing the necessary cooling. Beginning with this condition, the experiment runs were commenced. Midway through the experiment, the reactor

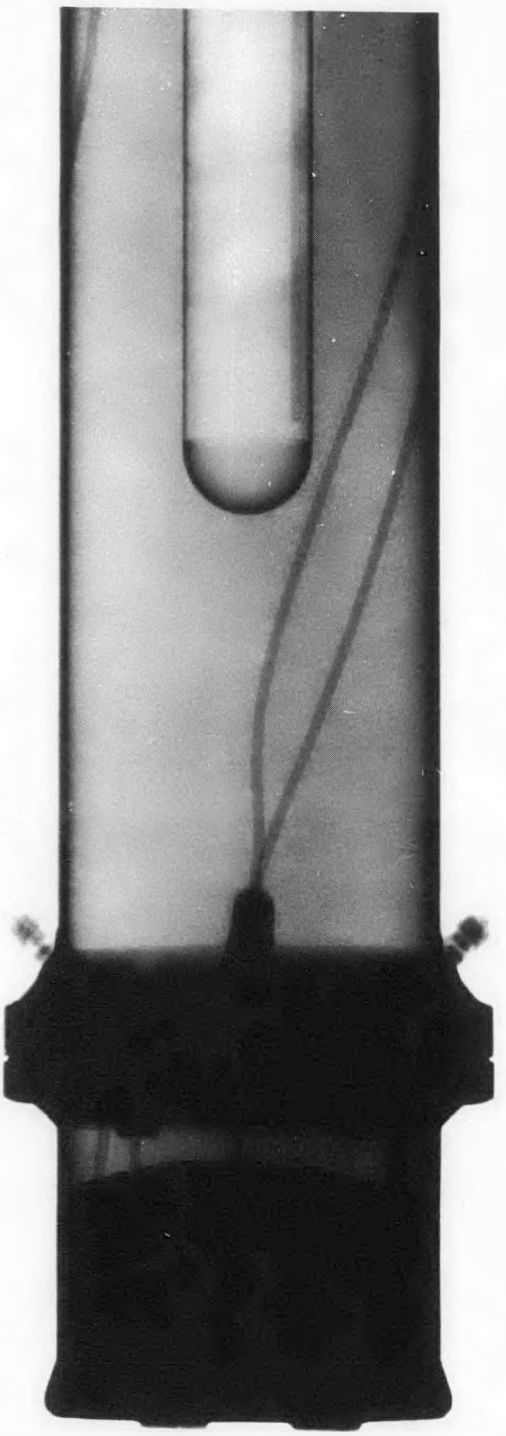

FIGURE 10 - X-ray of debris bed experiment capsule after filling.

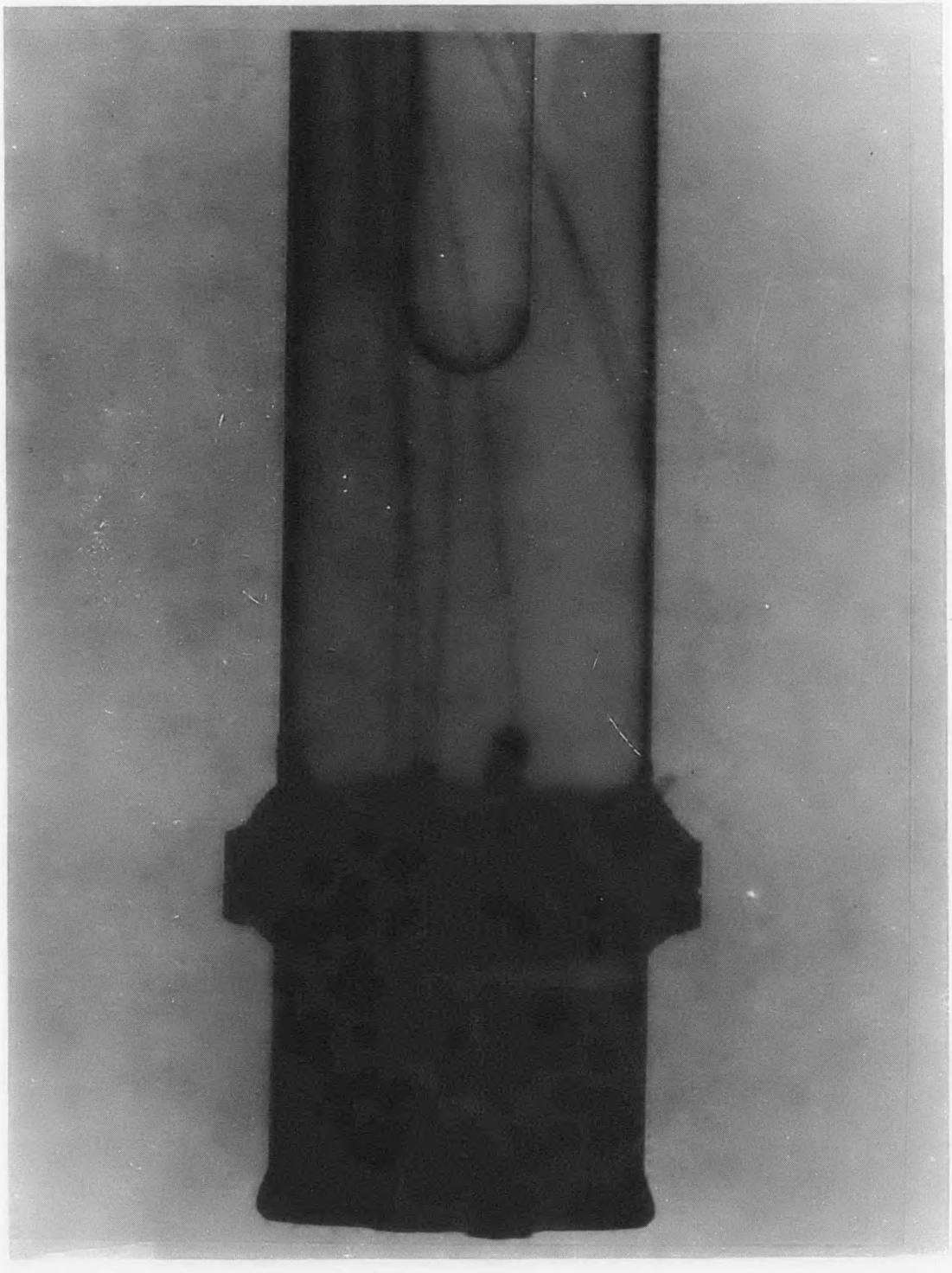

FIGURE 11 - X-ray of capsule taken at an angle 90° from Figure 10.

was shut down and the sodium was allowed to freeze. Then the experiment was brought up to power again and the runs repeated to test the effect of the freezing on the reproducibility of the data. A summary of the runs is given in the Appendix.

Based on the helium cooling loop measurements of experiment power, Figure 12 shows the relationship between ACPR power and experiment power. The data on experiment power given is formed by subtracting the bypass flow from the main loop flow to give the cooling flow. The reactor power is given by the operator's console instruments. The fairly large amount of scatter is caused primarily by errors induced by the small magnitude of the cooling flow. The line shown is a least squares fit, and shows a definite upward curvature. As is explained below in the Discussion section, this curvature is probably erroneous.

The matrix of conditions attained during the experiment is shown in Figure 13. Dryout conditions were not observed during the experiment. Higher power levels or higher temperatures than those shown could not be attained during the experiment due to limitations imposed by the use of a stainless steel capsule (follow-on experiments utilize Inconel 617 capsules).

Temperatures as determined from the three thermocouples in the liquid sodium above the bed showed time-varying oscillations of about $\pm$ 10 K which are presumably due to convective motion. Figure 14 shows the location of thermocouples in the bed. The "B" thermocouples are located on the bottom of the canister, while the "M" thermocouples are located 33 mm above the bottom. During

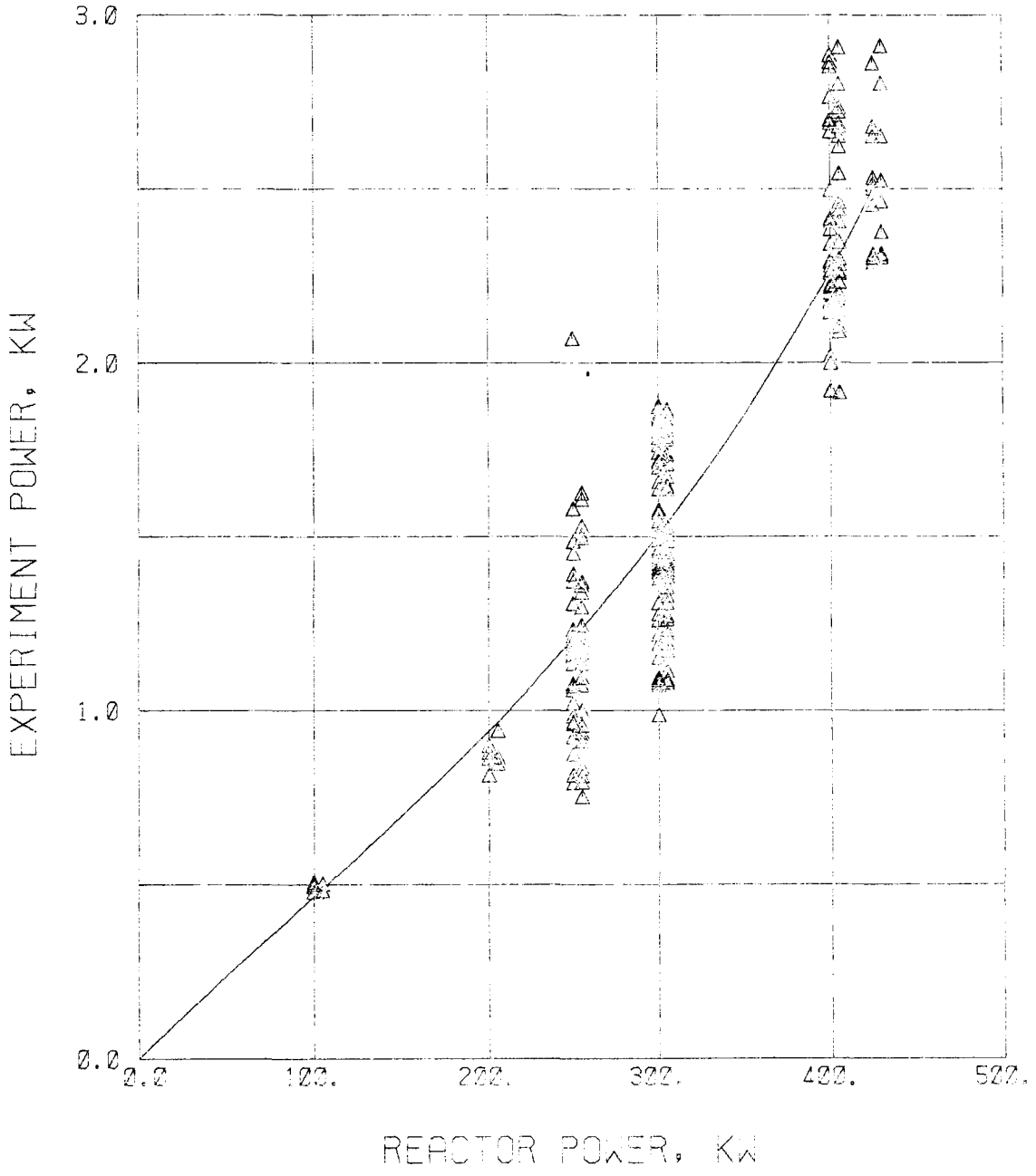

FIGURE 12 - Relationship between ACPR reactor power and experiment power (D-1).

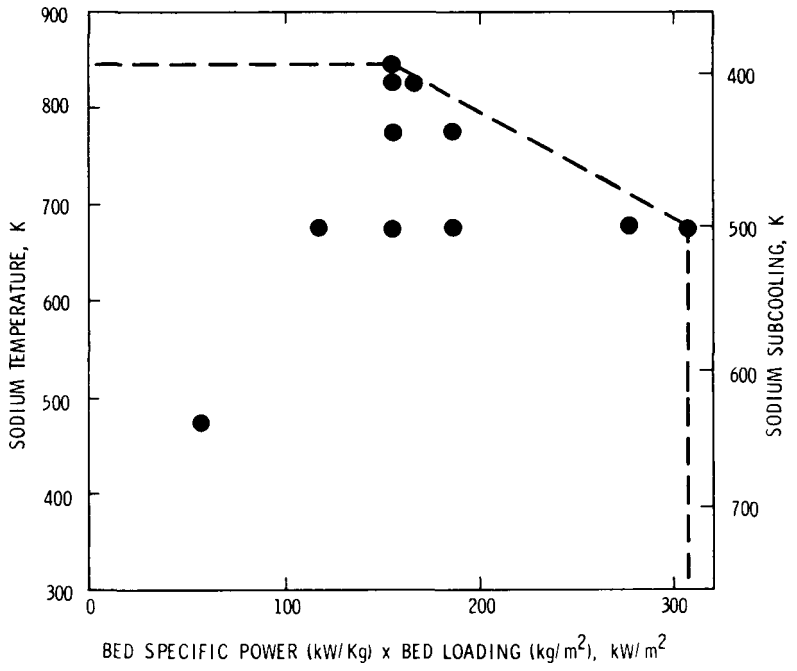

FIGURE 13 - Matrix of conditions attained during the experiment (bed loading 300 kg/m^2).

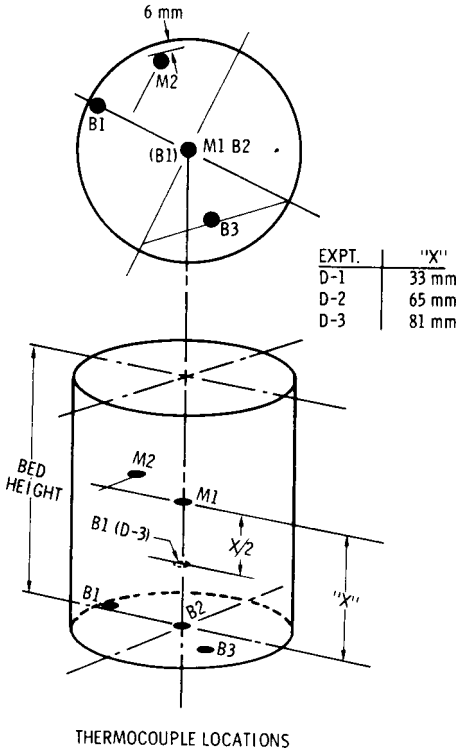

FIGURE 14 - Location of thermocouple junctions in the experiment.

the experiment, thermocouples B1 and B3 consistently gave equilibrium readings within 2 K of each other, despite B3 being an isolated junction thermocouple and B1 being a grounded junction thermocouple. Thermocouple B2 (grounded junction) initially gave readings which varied from 7 to 3 K below the average of B1 and B3. Thermocouple M2 gave readings which were consistently higher than M1 by amounts up to 14 K. Temperatures within the bed behaved, with one exception, smoothly and in a manner which characterizes thermal conduction. Conduction behavior is illustrated in Figure 15, in which temperature differences between thermocouples located on the bottom of the bed (B), and those located 33 mm higher (M), are plotted versus specific power. The straight line through the data corresponds to the application of the Fourier conduction equation for a heat-generating medium with an effective thermal conductivity of 31 W/m-K.

As the sodium temperature was being lowered to 673 K at constant power, after a number of hours of operation of the experiment, the signal from the thermocouple located in the lateral center at the bottom of the bed (B2) began a marked descent below the temperatures indicated by adjacent bottom thermocouples (B1, B3). After 1.5 hr it began to parallel the behavior of the sodium temperatures, except at a slightly higher temperature (Figure 16). Also during this period, the signal increasingly showed oscillatory behavior remarkably similar to the oscillations observed on the three thermocouples located in the sodium above the bed. Additional tests tend to indicate that this thermocouple was functioning

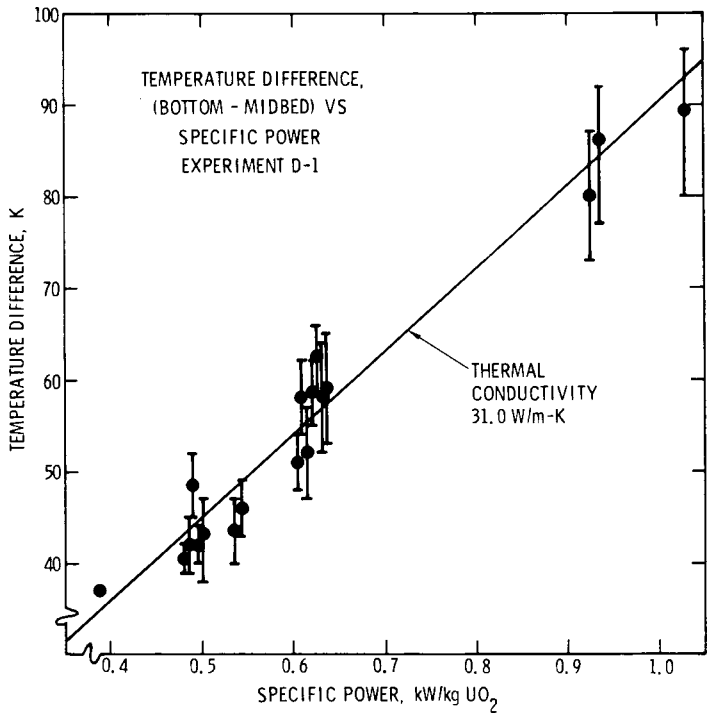

FIGURE 15 - Vertical temperature differences in the bed versus experiment specific power. The straight line corresponds to the Fourier conduction equation for a heat generating medium with an effective thermal conductivity of 31 W/m-K.

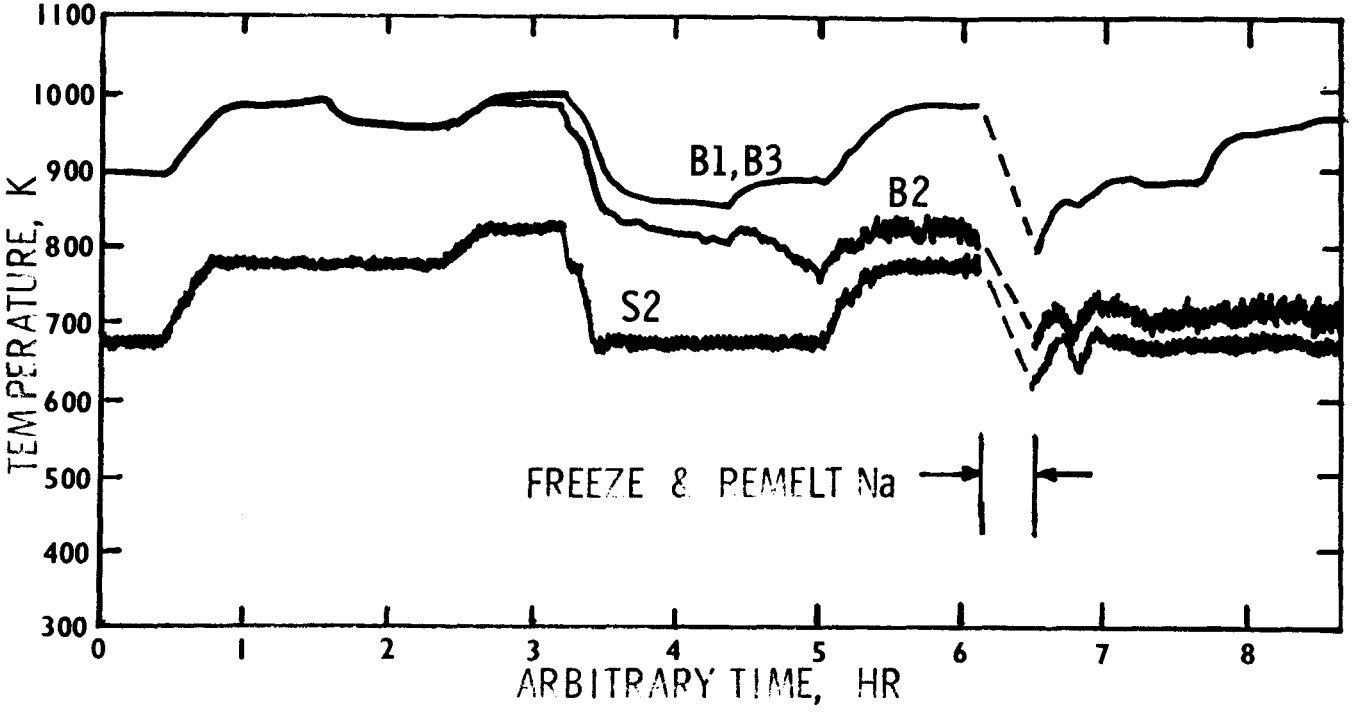

FIGURE 16 - Tracing of thermocouple signals showing transition of B2 temperature at bed bottom from conduction regime (B1, B3) to convection regime paralleling sodium temperatures above bed (S2). Sodium was frozen and remelted during the gap indicated (gap not to scale).

correctly. The adjacent thermocouples remained unaffected by this behavior throughout the remainder of the experiment.

A closer look at the conduction mode of bed heat transfer is afforded by Figure 17, which shows effective conductivity versus average bed temperature. The conductivity was calculated from the Fourier equation for a heat-generating medium using the differences between average temperatures at the bottom and averages at the level 33 mm above the bottom. Each abscissa datum represents the arithmetic mean of the average temperatures at each level. The extremes of the error bars represent the conductivity calculated using the minimum and maximum differences in temperature between the two levels. The calculation includes only the (early) data from thermocouple B2 which appears to correspond to conduction behavior. The straight line is a least-squares fit of the data. It has a positive slope.

DISCUSSION

Based upon work by previous investigators[14,15], dryout was not expected during D-1, even if the specific power of 1.25 kW/kg of UO_2 corresponding to 600 kW (ACPR) had been achieved (1.03 kW/kg of UO_2 was actually attained). Supplementary estimates by two principal investigators[16,17] have additionally predicted that dryout would not occur during D-1. In one of these supplementary estimates, theoretical account was taken of the sodium subcooling present in the Sandia experiments. Of the debris bed experiments in sodium so far reported, only three subcooled tests appear.[18] The remainder of the tests were performed at or near saturated conditions. The

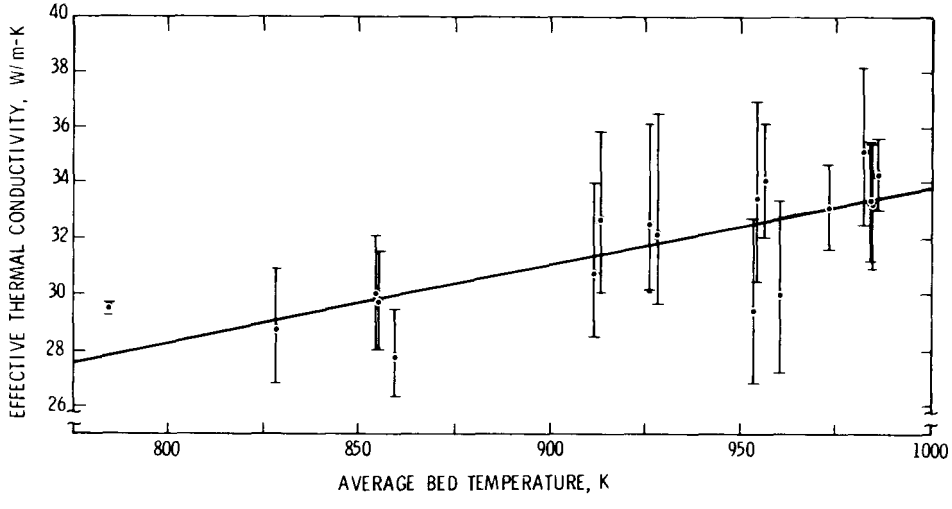

FIGURE 17 - Effective thermal conductivity of the bed versus average bed temperature. The straight line is a least-squares fit to the data.

subcooled tests were performed using an external heat source to heat the bottom of the container. While the present experiments more closely match expected reactor conditions, comparison with previous tests may be less direct, although the subcooling in the previous experiments was reported to have a negligible effect on dryout.

Lapwood,[19] Gasser and Kazimi,[20] Buretta and Berman,[11] and Hardee and Nilson[10] considered natural convection in a single-phase fluid in porous media under conditions that lead to instability in the otherwise stagnant fluid; i.e., the onset of convection. Corresponding critical Rayleigh numbers--one proportional to the heat generation rate, and the other to the difference in temperature between the upper and lower boundaries--are noted which demarcate the unstable (convective) and the stable (conductive) regimes. When applied to the Sandia experiments, these stability criteria predict a large region of stability; i.e., no single phase convection should occur. This may imply that most of the convective results reported previously by debris bed experimenters is two-phase convection occurring at internal (heat generation rate) Rayleigh numbers much below the single-phase critical value. (External (ΔT) Rayleigh numbers in previous experiments have been limited to small values by the small amounts of subcooling employed.)

Based on the permeability values determined as described above, Rayleigh numbers have been calculated for relevant debris bed experiment configurations and conditions. Comparisons with conventional, constant-viscosity, critical Rayleigh numbers indicate that the onset of single-phase convection would occur at power

levels much greater than those which characterize the onset of boiling in a conducting bed. This suggests that two-phase convection effects would tend to precede, and possibly preclude the occurrence of single-phase convection, and may even dominate bed behavior. However, recent analyses[21,22] of the onset of single-phase convection in water-saturated porous media with a large imposed temperature gradient have shown that the critical Rayleigh number is substantially reduced from the value predicted by a constant viscosity calculation due to the decrease of viscosity near the lower (hot) boundary. Similar analyses for sodium should show the same trend, since its viscosity also decreases with increasing temperature. A large reduction in critical Rayleigh number would nevertheless be required to support the inference of the onset of single-phase convection in preboiling beds of the D-series type.

Figure 18 compares the bed temperature data from this experiment with a heat transfer model which couples thermal conduction within the bed to natural convection in the liquid sodium above the bed. The correlation of McDonald and Connally[23] has been used to derive the boundary layer temperature drop, and a constant value of effective thermal conductivity in the bed has been chosen corresponding to the average value found above (Fig. 15). The deviations which are evident appear to be systematic, and it is believed that they are due to errors in the experiment power diagnostic. Specifically, the upward curvature in the relationship between experiment power and reactor power shown in Figure 12 is probably faulty. Substitution of a reasonable linear relationship for the curve

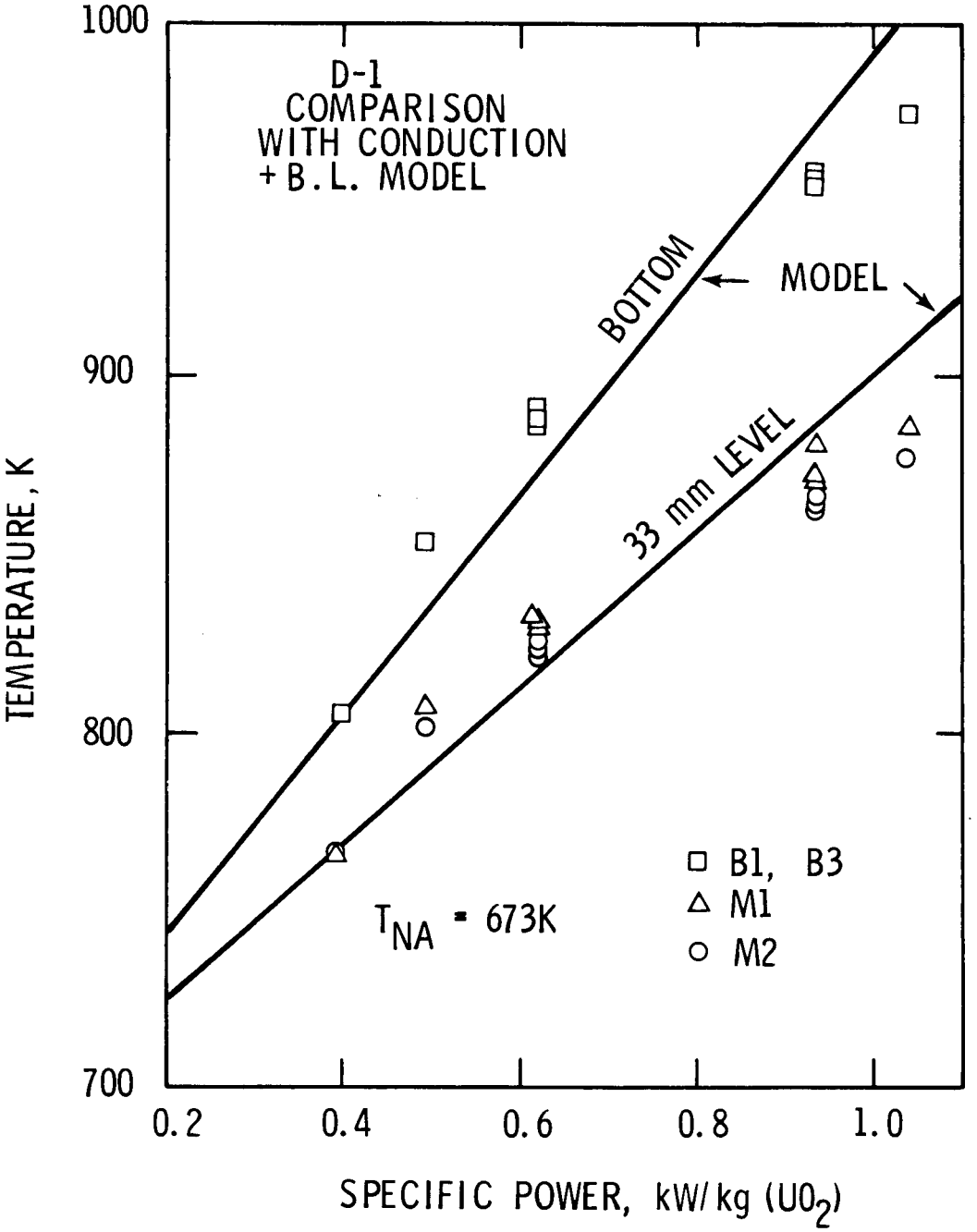

FIGURE 18 - Comparison of temperature data at a bulk sodium temperature of 673 K with the coupled conduction-convection model.

shown in that figure would remove most of the non-linearity visible in Figure 18 without substantially changing the derived value of effective thermal conductivity.

A recently published analysis[24] investigates the effect of sodium subcooling on the onset of boiling in a porous bed. For an adiabatic condition similar to that which occurs in the present experiment, the bed depth for incipient sodium boiling is calculated from

$$L = -\frac{k_B}{h} + \left[\frac{k_B^2}{h^2} + \frac{2k_B(\Delta T_{Sub})}{Q'}\right]^{1/2}$$

where k_B is the equivalent conductivity of the bed, h is the upward facing heat transfer coefficient, ΔT_{sub} is the subcooling, and Q' is the volumetric heat source strength. At a decay heat level which is stated to be 1 percent of full LMFBR power, the authors give resulting bed depths for incipient boiling which are less than 58 mm for sodium temperatures above 673 K (400°C). These predictions appear to be extremely conservative when compared with the results of the present experiment, which was subcooled (at the bottom of the bed) by more than 200 K at maximum power with a bulk sodium temperature of 673 K.

The effective thermal conductivity represented by the straight line in Figure 17 shows a positive slope. This contrasts with the trend of sodium conductivity, which shows decreasing values with increasing temperature in this range,[25] and may indicate some slight influence of convection at increasing bed temperatures.

The magnitude of the effective conductivity at 900 K is about half that of sodium alone at 900 K, which is not unexpected for a continuous medium which is 48 volume percent sodium. It is, however, somewhat in excess of the ~40 percent of sodium value that is calculated from from the frequently quoted equation given by Kampf and Karsten.[26]

Bed leveling effects are not expected in the absence of fluid motion within the bed. With the exception of the thermocouple B2 observations discussed above, no evidence supporting the existence of bed leveling fluid motions was found during the experiment.

CONCLUSIONS

An initial experiment simulating a 58 mm thick LMFBR fuel debris bed has been performed in liquid sodium in which the uranium dioxide particles composing the bed were internally heated by nuclear fission. Although the particle sizes were approximately uniformly distributed throughout the bed (a condition which may not typify the structure of a prototypic debris bed), care was exercised to ensure minimum packing in the formation of the bed, since substantial reduction in permeability can occur when uranium dioxide particles are gravitationally impacted from a height in a gas environment. The resultant particle bed had a porosity (sodium volume fraction) of 0.48. Its permeability, based upon measurements of similarly prepared UO_2, was probably close to 200 darcys.

The sodium conditions and specific power in the experiment are summarized in Figure 13. The dashed lines encompass sodium

conditions which characterize normal and off-normal operations of LMFBRs, and power levels typical of a decay heating curve from ~1 to 3 hours after shutdown onward if 100 percent retention of the fission products in the debris is assumed. Higher power and earlier times after shutdown are simulated if account is taken of gamma ray escape and if it is assumed that some fission products escape the fuel matrix during the LMFBR scenario.

The preponderant mode of heat transfer from the bed to the subcooled liquid sodium above the bed was thermal conduction through the bed. In this mode, the bed acts as a stationary conductor with negligible sodium convection. Its conductivity is about half the conductivity of pure sodium alone. On a smaller scale, the particle-to-fluid interface does not appear to offer significant resistance to heat transfer at the power levels tested. The heat transfer behavior of the bed was quite reproducible; even complete freezing and remelting of the sodium did not alter its behavior significantly.

The degree of temperature uniformity displayed by the thermocouples located at the same height in the bed tends to indicate small edge effects and uniform power generation, although the bed's temperature sensitivity to power nonuniformities is relatively low. The apparent lack of edge effects lends confidence to the necessary extrapolation to beds of larger lateral extent as required for application to the LMFBR post-accident scenario.

Subcooled liquid sodium was employed throughout this experiment because of the generally held opinion that the sodium coolant

in an LMFBR vessel will not approach bulk saturation conditions, even following a relatively severe accident, and because of accumulating evidence that particle beds in strongly subcooled fluids behave quite differently than do beds in saturated liquids at the same power level, particularly with regard to particle fluidization, leveling, and channeling effects.

In the conduction mode of bed heat transfer, a limiting condition is not expected to arise prior to the occurrence of boiling at or near the bottom of the bed. Thus, application of the Fourier equation for thermal conduction in a heat-generating medium implies

$$Q'L^2 \leq 2k_B\Delta T_{Sub}$$

where ΔT_{Sub} is the quantity $(T_{Boiling} - T_{Bulk})$. Implementation of this equation as a limiting condition for debris bed cooling yields values larger than those computed previously by others. However, the implication of saturation conditions at the bottom of the bed suggests that the temperature of the structure underlying a LMFBR debris bed may approach the local boiling temperature of sodium, with an attendant reduction in strength of the supporting structure.

The limited occurrence of a temperature signal during the experiment which can be interpreted as indicating convection in one zone of the bed must, in light of the value of calculated Rayleigh numbers, be viewed as anomalous pending additional analysis, further tests of the thermocouple, and detailed inspection of the convection site during the post-experiment examination.

NONEMCLATURE

C	Specific Heat
D	Bed Diameter
h	Heat Transfer Coefficient
k	Thermal Conductivity
L	Bed Height
Nu	Nusselt Number
Q' , Q'_v	Heat Generation Rate (bed volume, solid volume)
Ra , $\underline{Ra}$	Rayleigh Numbers
T_B, T_C	Temperature (bottom, top)
$\mathscr{L}$	Latent Heat of Vaporization
ϵ	Porosity
κ	Permeability
ν	Kinematic Viscosity
ρ	Density

Subscripts

B	Bed
C	Critical
ℓ	Liquid
v	Vapor

ACKNOWLEDGEMENT

A number of Sandia Laboratories' personnel made significant contributions to this work. Outstanding contributors not already noted include D. N. Cox (Mechanical Design and Technical Support), D. J. Sasmor (UO_2 and Sodium), S. N. Burchett (Stress Analysis), A. R. Phillips (Electronic and Electrical Design and Data Analysis), D. O. Lee (Out-of-pile Studies), I. C. Wilson (MRL) and L. E. Maxey (Assembly and Testing), S. M. Falacy and C. Csinnjinni (Fabrication, Calibration, and Maintenance), the experiment operating crews, and the operating staff of the ACPR.

REFERENCES

1. J. B. Rivard, "First In-Reactor Experiment with Simulated LMFBR Debris Bed," 1977 Winter Meeting ANS, Transactions, 27, p. 653-4.

2. B. F. Estes, F. M. Morris, J. C. Conant, and J. B. Rivard, Sandia Annular Core Pulse Reactor (ACPR) Safety Analysis Report, Sandia Laboratories Report No. SLA-73-0687, 1976.

3. J. A. Brammer, "Mobile Helium Cooling Loop System for In-Reactor PAHR Experiments," 1977 Winter Meeting ANS, Transactions, 27, p. 651-3.

4. R. R. Berlint and J. L. Krone, Sandia Executive: User's Manual, Sandia Laboratories Report SC-M-70-729B.

5. E. E. Lewis and R. Pfeffer, "The Influence of Source Geometry on Fission-Fragment Escape Properties," Nuclear Science and Engineering, 27, 581-85, (1967).

6. Charles P. Verdon and Richard L. Brehm, "Numerical Calculation of Gamma Ray Debris Bed Heating and Subsequent Temperature Distributions of Various Debris Bed Thicknesses and Compositions," Dept. of Nuclear Engineering, University of Arizona, Tucson, 1976.

7. Richard J. Bard (Los Alamos Scientific Laboratory), private communication to Daniel J. Sasmor (Sandia Laboratories), Nov. 18, 1976.

8. Thomas R. Rehm, University of Arizona, private communication to Joseph B. Rivard, "Analysis of Results," Oct. 15, 1976.

9. John M. Dengler, Permeability Studies with Uranium Dioxide Granules, Dept. of Chemical Engineering, University of Arizona, Tucson, Arizona, 1976.

10. H. C. Hardee and R. H. Nilson, Natural Convection in Porous Media with Heat Generation, SAND76-5904, Sandia Laboratories, 1976.

11. R. J. Buretta and A. S. Berman, ASME J. Appl. Mech., 98, 2 (1976).

12. W. Sun, "Convection Instability in Superposed Porous and Free Layers" Ph.D. Dissertation, U. of Minnesota (1973).

13. Howard G. Plein, private communication, 1976.

14. L. Baker, Jr., et al., Post-Accident Heat Removal in Fast Reactors, Argonne National Laboratory Report No. ANL/RAS 75-44, 1975.

15. V. K. Dhir and I. Catton, Study of Dryout Heat Fluxes in Beds of Inductively Heated Particles, NUREG-0262, University of California at Los Angeles for the U. S. Nuclear Regulatory Commission, 1977.

16. L. Baker, Jr., private communication to Richard L. Coats, December 27, 1976.

17. Vijay K. Dhir, private communication to Richard L. Coats, March 29, 1977.

18. J. C. Gabor, E. S. Sowa, L. Baker, Jr., J. C. Cassulo, "Studies and Experiments on Heat Removal from Fuel Debris in Sodium," ANS Fast Reactor Safety Meeting, April 3, 1974. CONF-740401-P2, pp. 823-844.

19. E. R. Lapwood, "Convection of a Fluid in a Porous Medium," Proc. Camb. Phil. Soc., 44, 508-521 (1948).

20. R. Gasser and M. Kazimi, "Onset of Convection in an Internally Heated Porous Medium," ANS Winter Annual Meeting, San Francisco, CA, November 16-21, 1975; ANS Transactions Vol. 22, TANSAO 22 1-836, pp. 446-447.

21. D. R. Kassoy and A. Zebib, "Variable Viscosity Effects on the Onset of Convection in Porous Media," Physics of Fluids, 18, No. 12 (1975).

22. A. Zebib and D. R. Kassoy, "Onset of Natural Convection in a Box of Water-Saturated Porous Media with Large Temperature Variation," Physics of Fluids, 20, No. 1 (1977).

23. J. S. McDonald and T. J. Connolly, "Investigation of Natural Convection Heat Transfer in Liquid Sodium," Nuclear Science and Eng. 8, 369-377 (1960).

24. M. S. Kazimi, S. S. Tsai, and R. D. Gasser, Post-Accident Fuel Relocation and Heat Removal in the LMFBR, BNL-NUREG-50603, 1977.

25. G. H. Golden and J. V. Tokar, "Thermophysical Properties of Sodium," ANL-7323 (1967).

26. H. Kampf and G. Karsten, "Effects of Different Types of Void Volumes on the Radial Temperature Distribution of Fuel Pins," Nuclear Application and Technology, Vol. 9, No. 3, p. 288 (Sept. 1970).

APPENDIX

BASIC DATA SUMMARY (D-1)*

THERMOCOUPLE READINGS (DEG C)

TIME	ACPR POWER (kW)	SODIUM (S2)	B1	B2	B3	M1	M2
1800	200	400	530	530	530	493	493
1946	400	400	683	677	682	600	591
2053	425	400	700	693	700	613	604
2140	300	400	618	618	617	558	552
2248	300	500	711	708	710	655	646
2338	250	500	679	673	678	635	632
0033	250	550	722	(703)	720	680	678
0126	250	400	580	(537)	579	534	528
0209	300	400	610	(507)	610	556	548
0315	300	500	708	(548)	706	659	651
----------SODIUM FROZEN AND REMELTED----------							
1032	300	400	611	(450)	611	556	549
1122	400	400	680	(436)	680	607	593
1240	300	500	708	(528)	709	660	655
1301	300	500	716	(515)	716	664	652
1350	270	550	731	(575)	730	690	684
1358	270	550	734	(570)	733	690	685
1431	250	565	732	(577)	731	692	687
1434	250	570	734	(585)	733	694	692

* Continuous analog recordings were maintained in addition to these discrete data points. B2 readings with parentheses are explained in text.